

ORIGINAL COPY  
FILE

A NUMERICAL STUDY OF TURBULENT  
HEAT TRANSFER IN A SPHERICAL ANNULUS

Werner Stein  
Harry Brandt

ASME Journal of Heat Transfer



December 1987

Lawrence  
Livermore  
National  
Laboratory

This is a preprint of a paper intended for publication in a journal or proceedings. Since changes may be made before publication, this preprint is made available with the understanding that it will not be cited or reproduced without the permission of the author.

#### DISCLAIMER

This document was prepared as an account of work sponsored by an agency of the United States Government. Neither the United States Government nor the University of California nor any of their employees, makes any warranty, express or implied, or assumes any legal liability or responsibility for the accuracy, completeness, or usefulness of any information, apparatus, product, or process disclosed, or represents that its use would not infringe privately owned rights. Reference herein to any specific commercial products, process, or service by trade name, trademark, manufacturer, or otherwise, does not necessarily constitute or imply its endorsement, recommendation, or favoring by the United States Government or the University of California. The views and opinions of authors expressed herein do not necessarily state or reflect those of the United States Government or the University of California, and shall not be used for advertising or product endorsement purposes.

A NUMERICAL STUDY OF TURBULENT  
HEAT TRANSFER IN A SPHERICAL ANNULUS

Werner Stein\*  
Harry Brandt\*\*

December 1987

\* Associate Member ASME  
Engineer  
Lawrence Livermore National Laboratory  
P. O. Box 808  
Livermore, California 94550

\*\* Member ASME  
Professor  
Mechanical Engineering Dept.  
University of California, Davis  
Davis, California 95616



# ABSTRACT

A numerical study of steady, buoyant, incompressible water flow and heat transfer through a spherical annulus has been made. A two dimensional computer code based on the TEACH code was rewritten in spherical coordinates to model the Navier-Stokes equation and to model fluid turbulence with a  $k-\epsilon$  turbulence model. Results are given for the total system Nusselt number, local heat transfer rate and fluid flow characteristics for both buoyant and non-buoyant laminar and turbulence modeled flow. Incorporating both the turbulence model and buoyancy into the calculations improves the results.

This work was performed under the auspices of the U.S. Department of Energy by Lawrence Livermore National Laboratory under contract No. W-7405-Eng.-48.



# NOMENCLATURE

A	surface area of inner sphere
$C_\mu, C_1, C_2$	coefficients in turbulence model
$C_p$	specific heat at constant pressure
E	von Karman constant
g	acceleration of gravity
$g_r$	acceleration of gravity in radial direction
$g_\theta$	acceleration of gravity in longitudinal direction
h	heat transfer coefficient
k	turbulent kinetic energy per unit mass
K	thermal conductivity of fluid
m	fluid mass flow rate
$NU_g$	total system Nusselt number
P	mean generation rate of turbulent kinetic energy per unit mass
$P_*$	heat transfer P - function
p	pressure
$q_w$	wall heat flux
r	radial coordinate
$r_i$	outside radius of inner sphere (= 0.1397 meters)
$r_o$	inside radius of outer sphere (= 0.1683 meters)
$R_i$	Richardson number ( $= \beta g (r_o - r_i) (T_{in} - T_{out}) / v_{in}^2$ )
$Re$	gap Reynolds number ( $= \rho U_A (r_o - r_i) / \nu$ )
T	temperature
$T_A$	average radial temperature
$T_i$	average temperature of inner sphere surface

$T_B$	bulk fluid temperature ( $= (T_{in} + T_{out})/2$ )
$T_W$	wall temperature
$U$	mean longitudinal velocity
$U_A$	average velocity at equator
$U_*$	friction velocity ( $= (\tau_w/\rho)^{1/2}$ )
$V$	mean radial velocity
$y$	distance from wall
$y^+$	dimensionless wall distance ( $= y k_p^{1/2} / \nu$ )
$\beta$	water volume coefficient of expansion
$\Gamma$	effective diffusivity
$\epsilon$	dissipation rate of turbulent kinetic energy per unit mass
$\theta$	longitudinal coordinate
$\kappa$	von Karman constant
$\mu$	dynamic viscosity
$\mu_T$	turbulent viscosity
$\nu$	kinematic viscosity
$\tau_w$	wall shear force
$\rho$	density
$\sigma$	Prandtl number
$\sigma_k, \sigma_\epsilon, \sigma_T$	turbulent Prandtl numbers for diffusion of $k$ , $\epsilon$ , and $T$
$\phi$	variable

### Subscripts

in	values at inlet region
e	values at the edge of cell adjacent to the wall
out	values at exit region
p	values at node point adjacent to wall
v	values at the edge of the viscous sublayer



## INTRODUCTION

The objective of this study is to predict the heat and momentum transfer of fluid flow through a spherical annulus. This problem is of interest in the temperature control of gyroscope gimbals, the cooling of spherical fuel elements in homogeneous nuclear reactors, and the guard cooling of spherical containers.

The problem analyzed involves the upward flow of water vertically into the annulus space between two concentric spheres as shown in Fig. 1. As the fluid enters the annulus and begins flowing around the spherical shape, its cross-sectional area increases considerably which in turn decreases its fluid velocity. The fluid decreases in velocity until it reaches the equator. After the equator, the fluid velocity increases as the flow cross-sectional area decreases. The fluid flow pattern exhibits a recirculation zone along the outer sphere in the entry region due to the sharp corner where the entrance pipe joins the annulus. The flow also exhibits changing patterns as it moves along the annulus. The flow exhibits aspects of a stagnation flow on the inner sphere upon entering, a boundary layer jet flow along the inner sphere as the fluid flows toward the equator, and then separation of the boundary layer along the inner sphere with a resultant recirculation region downstream of the separation point. In the region downstream of the equator, the flow assumes a velocity profile similar to that in the space between flat plates.

In this study the inner sphere is maintained at a temperature near zero degrees centigrade, and the outer sphere is insulated. The fluid entering is water at a temperature of  $50^{\circ}\text{C}$ . The water cools as it flows around the annulus and exits at the top. The water temperature is coolest near the inner sphere with the majority of heat transfer occurring in the entrance region along the inner sphere. The cooled fluid along the inner sphere generates buoyancy forces that retard the flow and may cause boundary layer separation.

Theoretical studies of flow through a spherical annulus have been reported by several investigators. Cobble (1963) assumed a simplified tangential velocity distribution and then calculated heat transfer based on the energy equation. Bird et al. (1964) presented the solution to isothermal creeping flow in a spherical annulus. Astill (1976) analyzed laminar forced convection flow with simplified boundary layer assumptions for air flowing between isothermal spheres. Ramadhyani et al. (1983) and Tuft and Brandt (1982) analyzed laminar forced convection in a spherical annulus without considering buoyancy-driven natural convection. Brown (1967) analyzed natural convection flow in a closed spherical annulus, and Ramadhyani et al. (1984) analyzed combined natural and forced convection laminar flow at low gap reynolds numbers.

Experimental studies have been reported by many investigators for various combinations of sphere and annulus sizes. Ward (1966) and Bozeman and Dalton (1970) provided a flow visualization study of isothermal flow in a spherical annulus. Rundell et al. (1968)

observed a flow rate independent separation point located approximately  $45^\circ$  downstream from the inlet along the inner sphere. Upstream of the separation point, the flow is characterized by a high-velocity jet of fluid along the inner sphere with a relatively low-velocity return flow along the outer sphere. The region of high velocity jetting fluid upstream of the separation point is a region of high heat transfer. Beyond the separation point, a return flow eddy is followed by a relatively tranquil flow. This region exhibits a relatively low heat transfer rate. Rundell measured temperature profiles and total heat transfer for steady flow for two sets of sphere sizes. Astill et al. (1978) and Newton (1977) investigated spherical annulus flow and heat transfer experimentally. They presented a correlation based on total heat transfer measurements. Tuft and Brandt (1982) investigated spherical annulus flow for the case of a constant temperature inner sphere and an adiabatic outer sphere. They measured local and total heat transfer as well as temperature profiles and separation point location. They also analyzed laminar non-buoyant flow through an annulus configuration shown in Fig. 1.

In this paper an extensive numerical study of spherical annulus fluid flow is presented with detail comparisons with the experimental data of Tuft and Brandt (1982). The laminar analysis is extended by incorporating the effects of buoyancy. The analyses were further extended by modeling the fluid turbulence with a two-equation ( $k-\epsilon$ ) turbulence model. This work is believed

to be the first two-dimensional analysis of the full Navier-Stokes equations with a  $k-\epsilon$  turbulence model for steady, incompressible, spherical coordinate fluid flow and convective heat transfer. This work evaluates the  $k-\epsilon$  turbulence model by comparing it with experimentally determined total Nusselt numbers, with local heat transfer rates, with temperature profiles and with inner sphere boundary layer separation point locations. Ranges of fluid flow for gap Reynold's numbers,  $Re$ , of 110 to 1086 were investigated with water entering the annulus at  $50^\circ\text{C}$  and with convective cooling caused by a nominally  $0^\circ\text{C}$  inner sphere. The Richardson number,  $R_i$ , for this flow varied from 0.001 to 0.4.

## **MATHEMATICAL AND PHYSICAL MODEL**

### Governing Equations

The numerical model is based on the solution of the steady two-dimensional incompressible form of the time-averaged Navier-Stokes equation, incorporating the Boussinesq turbulent-viscosity concept. The turbulent viscosity is calculated from the two-equation high Reynolds number form of the  $k-\epsilon$  turbulence model developed by Launder and Spalding (1974) and Chieng and Launder (1980). The governing equations in spherical coordinates may be written in the following general form:

$$\begin{aligned} & \frac{1}{r^2} \frac{\partial}{\partial r} (r^2 \rho V \phi) + \frac{1}{r \sin \theta} \frac{\partial}{\partial \theta} (\rho U \sin \theta \phi) \\ &= \frac{1}{r^2} \left[ \frac{\partial}{\partial r} \left( r^2 \Gamma \frac{\partial \phi}{\partial r} \right) + \frac{1}{\sin \theta} \frac{\partial}{\partial \theta} \left( \sin \theta \Gamma \frac{\partial \phi}{\partial \theta} \right) \right] + S_\phi \end{aligned} \quad (1)$$

where  $\phi$  represents the dependent variables of longitudinal velocity,  $U$ , radial velocity,  $V$ , fluid temperature,  $T$ , turbulent kinetic energy per unit mass,  $k$ , and dissipation rate of turbulent kinetic energy per unit mass,  $\epsilon$ . A summary of these equations is given in Table 1. The constants applicable to the  $k$  and  $\epsilon$  transport equations are given in Table 2.

#### Near-Wall Model

Viscous effects, due to the no-slip condition on the smooth spherical walls, are very influential on the flow. Within the near-wall boundary layer, the velocity typically follows a logarithmic law behavior. Two versions of the high Reynold's number form of the  $k$ - $\epsilon$  turbulence model were evaluated.

The version of Launder and Spalding (1974) gives the relationship between the velocity at the node adjacent to the wall and shear stress,  $\tau_w$ , as:

$$\frac{U_p}{\tau_w/\rho} C_\mu^{1/4} k_p^{1/2} = \frac{1}{\kappa} \ln \left[ E y_p \frac{(C_\mu^{1/2} k_p)^{1/2}}{\nu} \right]. \quad (2)$$

This relationship should be applied at a dimensionless wall distance,  $y^+$ , whose values are in the range  $20 < y^+ < 200$ . At values of  $y^+ \leq 20$ , the flow is assumed laminar. The dissipation,  $\epsilon$ , at the first node adjacent to the wall is evaluated by:

$$\epsilon_p = \frac{C_\mu^{3/4} k_p^{3/2}}{y_p} \quad (3)$$

and the average value of  $\epsilon$  over the control volume at the wall is evaluated by:

$$\int_0^{y_p} \epsilon dy = C_\mu^{3/4} \frac{k_p^{3/2}}{\kappa} \ln \left[ E y_p \frac{(C_\mu^{1/2} k_p)^{1/2}}{\nu} \right]. \quad (4)$$

The second version of the  $k$ - $\epsilon$  model evaluated is that of Chieng and Launder (1980). Figure 2 shows the assumed approach where the control volume around the wall adjacent node  $p$  contains a viscous sublayer out to a distance  $y_v$  from the wall, and the turbulent kinetic energy varies linearly from the node adjacent to the wall to  $y_v$ . The connection between the velocity at the node adjacent to the wall and the wall shear stress,  $\tau_w$ , is given by:

$$\frac{U_p C_\mu^{1/4} k_v^{1/2}}{\tau_w / \rho} = \frac{1}{\kappa} \ln \left[ E y_p \frac{(C_\mu^{1/2} k_v)^{1/2}}{\nu} \right] \quad (5)$$

with the kinetic energy of turbulence,  $k$ , evaluated at the edge of the viscous sublayer.

The dissipation,  $\epsilon$ , is again evaluated at the first nodal point adjacent to the wall by:

$$\epsilon_p = \frac{C_\mu^{3/4} k_p^{3/2}}{y_p}. \quad (6)$$

Other models in the near wall region for  $\epsilon$ , in the  $\epsilon$ -equation, were considered. The Amano and Jensen (1982) two layer model, as applied to impinging jet flow, showed little improvement in heat transfer over the Chieng and Luander (1980) model. The Amano (1984) two and three layer models, as applied to

an abrupt pipe expansion case, did show a significant improvement. Heat transfer in our spherical annulus occurs only on the inner sphere and represents a case similar to impinging jet flow and thus the Amano and Jensen (1982) model is expected to give similar results compared to the model by Chieng and Launder (1980).

The mean generation rate,  $P$ , of the turbulent kinetic energy at the first node adjacent to the wall is given by:

$$P = \frac{\tau_w (U_e - U_v)}{y_e} + \frac{\tau_w (\tau_e - \tau_w)}{\rho C_\mu \frac{y_e}{k_v^{1/2}} y_e} \left(1 - \frac{y_v}{y_e}\right) \quad (7)$$

and the mean dissipation rate,  $\epsilon_m$ , is given by:

$$\epsilon_m = \frac{2k_v^{3/2}}{y_e R_v} + \frac{1}{2.55y_e} \left[ \frac{2}{3} (k_e^{3/2} - k_v^{3/2}) + 2a(k_e^{1/2} - k_v^{1/2}) + \lambda \right] \quad (8)$$

where

$$\lambda = a^{3/2} \ln \left[ \frac{(k_e^{1/2} - a^{1/2})(k_v^{1/2} + a^{1/2})}{(k_v^{1/2} - a^{1/2})(k_e^{1/2} + a^{1/2})} \right] \text{ if } a > 0 \quad (9)$$

$$= 2(-a)^{3/2} \left[ \tan^{-1} \frac{k_e^{1/2}}{(-a)^{1/2}} - \tan^{-1} \frac{k_v^{1/2}}{(-a)^{1/2}} \right] \text{ if } a < 0 \quad (10)$$

and where

$$a = k_p - \frac{(k_p - k_E)}{(y_p - y_E)} y_p \quad (11)$$

and

$$R_v = \frac{y_v k_v^{1/2}}{v} = 20 . \quad (12)$$

The local wall heat flux and near wall temperature profile are given as:

$$\frac{\rho C_p C_\mu^{1/4} k_p^{1/2} (T_w - T_p)}{q_w} = \sigma_T \left[ \frac{1}{k} \ln \left( E y_p \frac{(C_\mu^{1/2} k_p)^{1/2}}{v} \right) + P_* \right] \quad (13)$$

where  $P_*$  is the P-function given by Jayatilleke (1969)

$$P_* = 9.24 \left( \sigma/\sigma_T \right)^{3/4 - 1} \left( 1 + 0.28 \exp(-0.007 \sigma/\sigma_T) \right) . \quad (14)$$

#### Numerical Solution Procedure

The method used for solving equation (1) is the solution procedure of the TEACH code, Patankar (1980). This program takes a control volume approach with scalar variables evaluated at the center of a control volume and the velocity vector quantities evaluated at the control volume boundaries. The TEACH code version used in this study uses a hybrid differencing scheme in which central differencing is used when the control volume Peclet number is less than 2 and upwind differencing is used for Peclet numbers greater than 2. The problem of determining the pressure distribution and satisfying mass conservation is overcome by adjusting the pressure field so as to satisfy mass conservation.

This method is the so-called semi-implicit method for pressure-linked equations (SIMPLE) algorithm.

For this study the TEACH code was rewritten from cylindrical coordinates into spherical coordinates. The energy equation to model the heat transfer was added as well as the near wall models for the  $k$ - $\epsilon$  equations.

At the inflow boundary region, a uniform temperature and velocity profile is given. The turbulence intensity ( $k/V_{in}^2$ ) is assumed to be in the range of 0.005, and the turbulent length scale ( $k^{3/2}/\epsilon$ ) is given by  $0.03 r_o$ . At the outflow boundary region, the flow is assumed to be of the parabolic type. The inner sphere temperature is specified and the outer sphere is assumed to be adiabatic. A no slip velocity boundary condition is applied at the sphere walls, and symmetry is assumed about the vertical centerline.

Computations for laminar flow were made primarily with a uniform mesh of 36 node points in the radial direction and 60 node points in the longitudinal direction. Under-relaxation of the conservation equations was required for convergence. Typically the momentum equations required a relaxation parameter of 0.5, and the pressure correction equation required relaxation parameters from 0.8 for non-buoyant flow to 0.2 for buoyant flows. Convergence occurred usually in less than 600 iterations, with one iteration representing a solution of each conservation equation. The convergency criteria were based on a normalized mass error balance, with convergence assumed for values below  $1 \times 10^{-5}$ . The balance was calculated by summing the absolute values of the mass

flow errors at each node point divided by the total mass flow rate. The computations were run on a CRAY-1 computer and, for a  $60 \times 36$  mesh, required approximately 2 minutes of computer time.

Mesh independence studies for laminar flow were made at  $Re = 110$ . Increasing the mesh longitudinally by 52% resulted in a 1% increase in total system Nusselt number,  $Nu_g$ , and the flow separation point shifted upstream by 3%. The mean longitudinal velocity,  $U$ , varied by 5% in the inlet region to less than 1% in the downstream regions. Increasing the mesh radially by 55% resulted in a 5% decrease in total system Nusselt number,  $Nu_g$ , and the flow separation point shifted downstream by 4%. The mean longitudinal velocity,  $U$ , varied by 4% in the inlet region to less than 1% in the downstream regions.

Computations for turbulent flow were made primarily using a mesh with 12 radial nodes and 60 longitudinal nodes. Under-relaxation of the conservation equations for turbulent calculations was also required. Typically the momentum equations required a relaxation parameter of 0.5, the pressure correction equation required relaxation parameters down to 0.2, and the  $k$  and  $\epsilon$  equations required relaxation parameters of 0.3. Applying a convergence criteria similar to that for laminar flow resulted in convergence after approximately 1500 iterations. Increasing the mesh longitudinally by 52% at  $Re = 1086$  resulted in a 2% decrease in total system Nusselt number,  $Nu_g$ . The mean longitudinal velocity,  $U$ , and turbulent kinetic energy,  $k$ , varied by 2% and 3% respectively in the inlet region. In the relatively quiescent downstream regions, the mean longitudinal velocity,  $U$ , varied by

3% and the turbulent kinetic energy,  $k$ , decreased as much as 14%. Increasing the mesh radially by 40% resulted in a 3% increase in total system Nusselt number,  $Nu_g$ . The longitudinal velocity,  $U$ , varied by less than 2%, throughout the flow. The turbulent kinetic energy,  $k$ , varied by 2% in the inlet regions to values decreased as much as 14% in the downstream regions. The computations were run on a CRAY-1 computer and, for a  $60 \times 12$  mesh, required approximately 2-1/2 minutes of computer time.

## RESULTS AND DISCUSSION

### Laminar Flow

Analysis of laminar flow through a heated spherical annulus, without buoyancy effects considered, was performed by Ramadhyani et al. (1983). Ramadhyani's analyses were duplicated in this study using the spherical coordinate version of the TEACH code in an effort to verify proper operation of the code. The results gave identical flow patterns with a recirculation zone along the wall of the outer sphere and separation of the flow along the wall of the inner sphere occurring approximately three-quarters around the sphere. Further work by Ramadhyani et al. (1984) in which the buoyancy effects were modeled showed a strong effect on the laminar flow patterns caused by buoyancy. Duplication of these calculations again produced identical flow patterns and showed that buoyancy effects may have a strong impact on heated flow in a spherical annulus.

Computational results were obtained for the total Nusselt number as a function of the gap Reynolds number for hot water flow

through the spherical annulus configuration shown in Fig. 1. The total Nusselt number,  $NU_g$ , is calculated from average inner sphere temperature, average inlet and exit temperatures, and the fluid mass flow rate by:

$$NU_g = \frac{mC_p (T_{out} - T_{in}) (r_o - r_i)}{A(T_i - T_B) K} \quad (15)$$

Results were obtained for laminar flow with and without buoyancy effects incorporated into the momentum equations. Figure 3 shows results for total system Nusselt number for laminar buoyant flow. The results show that the laminar buoyant model underpredicts the total Nusselt number by 16% at a gap Reynolds number of 110. At a gap Reynolds number of 1086 the total Nusselt number is overpredicted by 12%. For the non-buoyant laminar case, the total system Nusselt number is lower initially at a gap Reynolds number of 110 but soon increases and equals the values for the laminar buoyant case for gap Reynolds numbers of 180 and above. The results for both the laminar buoyant and non-buoyant cases show an improvement over results calculated by Tuft and Brandt (1982) as shown in Fig. 3. The calculations in this study for laminar flow were performed with a mesh that had 60 longitudinal nodes and 36 radial nodes, which is finer than the 16 radial nodes used by Tuft and Brandt (1982).

The calculational results for the location of the separation point of the boundary layer along the inner sphere are given in Fig. 4. The results for laminar non-buoyant flow, as well as the results of Tuft and Brandt (1982) for laminar non-buoyant flow,

show a separation point near  $80^\circ$  at a gap Reynolds number of 110. The separation point is located in a region of adverse pressure gradient with the experimental wall jet separating sooner than predicted due to observed vortex motion and flow instabilities. Incorporating the effects of buoyancy into the laminar calculations, however, shows in Fig. 4 that buoyancy has a marked effect on the location of the separation point. The cooling of the fluid on the inner sphere wall gives rise to negative buoyancy forces that act against the flow direction and thus aid in causing separation. Incorporating buoyancy improves the calculation of the location of the separation point at lower gap Reynolds numbers but does not affect the results at higher gap Reynolds numbers. The calculational results do show the trend of the separation point moving downstream with increases in gap Reynolds number.

Figure 5 shows calculated and experimental local heat transfer rates for gap Reynolds numbers of 110, 465, and 1086 for laminar buoyant flow. The maximum heat transfer rate occurs in the inlet region where maximum wall jet velocities occur on the inner sphere. The heat transfer rate decreases with increasing angle due to the deceleration of the wall jet. A local minimum heat transfer rate occurs at the location of the separation point where the velocity gradient is zero and the fluid is stagnant. Downstream of the separation point, a region of reverse flow exists and the heat transfer rate increases. The flow reattaches downstream of the separation point, and the heat transfer rate assumes a relatively flat profile in the downstream low-velocity

region. Also shown is the calculated local heat transfer rate for laminar non-buoyant flow at a gap Reynolds number of 110. At higher gap Reynolds numbers, the difference between buoyant and non-buoyant cases becomes small. The computed heat transfer rate in the inlet region is considerably underpredicted. Experimental observations show vortex motion, large temperature fluctuations, and unstable flow geometry in this region, which suggest that the flow is turbulent with an associated increased heat transfer rate.

Calculated profiles of normalized average radial temperature are shown in Fig. 6. For laminar buoyant flow the profile at a gap Reynolds number of 110 shows a profile that is much improved over the non-buoyant case. At higher gap Reynolds numbers of 465 and 1086, the profiles that are shown in Fig. 6 for laminar buoyant flow are also found to be very similar to the non-buoyant laminar case. The temperature profiles are very much dependent on the location of the separation point. Since a local minimum in heat transfer rate, velocity gradient, and temperature is associated with the separation point, the accuracy of these profiles improve as separation is more accurately predicted.

#### TURBULENT FLOW

The buoyant laminar flow analysis was extended by incorporating a  $k-\epsilon$  turbulence model (Launder and Spalding, 1974) to calculate a turbulent viscosity.

Calculational results for local heat transfer rate at gap Reynolds numbers of 110, 465, and 1086 are shown in Fig. 7. The results show a high local heat transfer rate in the entrance

region which falls rather sharply until it levels off to a fairly constant value in the quiescent regions of the flow. Comparing the turbulent calculations to the buoyant laminar flow results of Fig. 6 shows that the  $k$ - $\epsilon$  model results are improved in the entrance region and follow more closely the experimentally determined slope of the local heat transfer curve at gap Reynolds numbers of 465 and 1086. The higher heat transfer rates in the inlet region along the inner sphere are due to large velocity gradients in the wall jet. These large velocity gradients produce high turbulent kinetic energies and associated high turbulent viscosities and heat transfer coefficients. The wall jet velocity drops off rapidly as the equator is approached and results in an associated drop in turbulent heat transfer coefficient. The values of dimensional wall distance,  $y^+$ , vary considerably along the inner sphere wall. In the entrance region where a wall jet along the inner sphere exists, the values of  $y^+$  are initially very high and remain relatively high until either the flow approaches the equator or boundary layer separation occurs. Further downstream, the flow is relatively quiescent and  $y^+$  becomes smaller. At a high gap Reynolds of  $Re = 1086$ , the values of  $y^+$  vary from 233 to 43 in the first half of the annulus. In the annulus downstream of the equator, the values of  $y^+$  vary from 34 to 19. For a gap Reynolds number of 465, the values of  $y^+$  from the entrance to the separation point vary from 92 to 20, but downstream of separation the values of  $y^+$  are below 20, and the flow is assumed to be in the laminar sublayer.

Results for total Nusselt number based on a  $k-\epsilon$  turbulent flow analysis are also given in Fig. 3. For buoyant calculations the  $k-\epsilon$  model gives similar results when compared to the laminar buoyant analyses especially at high and low Reynolds numbers. The results for non-buoyant turbulent flow shown in Fig. 3 are not as accurate as those for buoyant flow at a Reynolds number of 110 but soon equal the buoyant turbulent case results at higher Reynolds numbers. The buoyant turbulent analysis, at  $Re = 110$ , predicts more accurately than the non-buoyant case the boundary layer separation on the inner sphere and thus results in a more accurate calculation of heat transfer. Applying the boundary conditions from the  $k-\epsilon$  model of Chieng and Launder (1980) gave total Nusselt number results that changed little from those of the Launder and Spalding (1974) model.

Normalized average radial temperature profiles based on turbulent flow are given in Fig. 8. The calculated profile at a gap Reynolds number of 1086 is more accurate than that at a low gap Reynolds number of 110. Comparing the turbulent calculation to the laminar buoyant flow calculation shows better agreement at a gap Reynolds number of 110 for laminar flow and better agreement for the  $k-\epsilon$  turbulence model at a gap Reynolds number of 1086. Figures 9 and 10 show typical calculated horizontal velocity and temperature profiles across the annulus at several locations for a gap Reynolds number of 260.

Results for the location of the separation point using the buoyant  $k-\epsilon$  model are shown in Fig. 4. The results fall between the data of the non-buoyant and the buoyant laminar cases. At

high gap Reynolds numbers, the buoyant  $k$ - $\epsilon$  model did not give any separation. Flow in the annulus up to the annulus equator experiences a positive pressure gradient along the boundary layer due to increasing cross-sectional area and decelerating fluid. Boundary layer separation occurs if the momentum of the boundary layer cannot overcome the pressure gradient. Downstream of the equator, a negative pressure gradient exists, and flows that have not yet separated will tend not to separate. The non-buoyant  $k$ - $\epsilon$  model calculation did not predict any separation occurring over the range of gap Reynolds number from 110 to 1086. In an attempt to obtain a better calculation of separation point location, a simple mixing length model ( $l_m = \kappa y_p$ ) was incorporated into the laminar analysis at the wall adjacent node. The results show in Fig. 4 that this mixing length model gives the best results over the range of gap Reynolds numbers considered.

## CONCLUSIONS

It is believed that this study is the first analysis in which the two equation  $k$ - $\epsilon$  turbulence model and the full axisymmetric Navier-Stokes equations have been applied to steady spherical annulus turbulent forced convection flow.

There are four main conclusions from this study of fluid flow and heat transfer in a spherical annulus:

1. Incorporating a two-equation  $k-\epsilon$  turbulence model improves the computation of local heat transfer over a laminar model calculation, especially in the entrance region where a high-velocity stream of fluid flows along the inner sphere wall.
2. Incorporating buoyancy into the computations shows that buoyancy forces are significant at lower gap Reynolds numbers and strongly affect both the fluid flow pattern and the location of the boundary layer separation point on the inner sphere.
3. The location of the separation point of the boundary layer along the inner sphere moves downstream with increases in the gap Reynolds number.
4. Predictions of the location of the boundary layer separation point along the inner sphere wall was more accurate at lower gap Reynolds numbers than at higher gap Reynolds numbers.

## REFERENCES

Amano, R. S. and Jensen, M. K., 1982, "A Numerical and Experimental Investigation of Turbulent Heat Transport of An Axisymmetric Jet Impinging on a Flat Plate," ASME Paper 82-WA/HT-55.

Amano, R. S., 1984, "Development of a Turbulence Near-Wall Model and its Application to Separated and Reattached Flows," Numerical Heat Transfer, Vol. 7, pp. 59-75.

Astill, K. N., 1976, "An Analysis of Laminar Forced Convection Between Concentric Spheres," ASME Journal of Heat Transfer, Vol. 98, pp. 601-608.

Astill, K. N., Kerney, P. J., and Newton, R. L., 1978, "An Experimental Investigation of Forced Convection Between Concentric Spheres at Low Reynolds Number," Proceedings of the Sixth International Heat Transfer Conference, 5, pp. 179-184.

Bird, R. B., Stewart, W. E., and Lightfoot, E. N., 1964, Transport Phenomena, John Wiley and Sons, New York, New York, pp. 117-118.

Bozman, J. D., and Dalton, C., 1970, "Flow in the Entrance Region of a Concentric Sphere Heat Exchanger," ASME Journal of Heat Transfer, Vol. 92, pp. 184-185.

Brown, J. R., 1967, "Natural Convection Heat Transfer Between Concentric Spheres," Ph.D. Dissertation, University of Texas, Austin, Texas.

Cobble, M. H., 1963, "Spherical Shell Heat Exchanger-Dirichlet Problem," Journal of the Franklin Institute, pp. 197-198.

Chieng, C. C. and Launder, B. E., 1980, "On the Calculation of Turbulent Heat Transfer Downstream From an Abrupt Pipe Expansion", Numerical Heat Transfer, Vol. 3, pp. 189-207.

Jayatilleke, C. L., 1969, "The Influence of Prandtl Number and Surface Roughness on the Resistance of the Laminar Sub-Layer to Momentum and Heat Transfer," Progress in Heat and Mass Transfer, Vol. 1, pp. 193-329.

Launder, B. E., and Spalding, D. B., 1974, "The Numerical Computation of Turbulent Flows", Computer Methods in Applied Mechanics and Engineering, Vol. 3, pp. 269-289.

Newton, R. L., 1977, "An Experimental Investigation of Forced Convection Between Concentric Spheres," Master's Thesis, Tufts University, Medford, Massachusetts.

Patankar, S. V., 1980, "Numerical Heat Transfer and Fluid Flow", Hemisphere Publishing Corp.

Ramadhyani, S., Torbaty, M., and Astill, K. N., 1983, "Laminar Forced Convection Heat Transfer in Spherical Annuli," ASME Journal of Heat Transfer, Vol. 105, pp. 341-349.

Ramadhyani, S., Zenouzi, M., and Astill, K. N., 1984, "Combined Natural and Forced Convective Heat Transfer in Spherical Annuli," ASME Journal of Heat Transfer, Vol. 106, pp. 811-816.

Rundell, H. A., Ward, E. G., and Cox, J. E., 1968, "Forced Convection in Concentric-Sphere Heat Exchangers," ASME Journal of Heat Transfer, Vol. 90, pp. 125-129.

Tuft, D. B., and Brandt, H., 1982, "Forced Convection Heat Transfer in a Spherical Annulus Heat Exchanger", ASME Journal of Heat Transfer, Vol. 104, pp. 670-677.

Ward, E. G., 1966, "Flow Through the Annulus Formed Between Concentric Spheres," Master's Thesis, University of Houston, Houston, Texas.

Table 1 Summary of Equations Solved.

Continuity	$\phi = 1$	$\Gamma = 0$	$S\phi = 0$
Energy	$\phi = T$	$\Gamma = \frac{\mu}{\sigma} + \frac{\mu_T}{\sigma_T}$	$S\phi = 0$
Turbulence energy	$\phi = k$	$\Gamma = \frac{\mu_T}{\sigma_K}$	$S_\phi = \rho P - \rho \epsilon$
Energy dissipation	$\phi = \epsilon$	$\Gamma = \frac{\mu_T}{\sigma_\epsilon}$	$S\phi = C_1 \frac{\epsilon}{k} P - C_2 \frac{\epsilon^2}{k}$

$$\text{U-Momentum} \quad \phi = U \quad \Gamma = \mu + \mu_T \quad S_\phi = -\frac{1}{r} \frac{\partial}{\partial \theta} p - \frac{\rho UV}{r} + \Gamma \frac{\partial}{\partial r} \left( \frac{U}{r} \right)$$

$$+ \frac{1}{r^2} \frac{\partial}{\partial r} \left( r \Gamma \left( U + \frac{\partial V}{\partial \theta} \right) \right) + \frac{\Gamma}{r^2} \frac{\partial V}{\partial \theta} + \frac{1}{r^2 \sin \theta} \frac{\partial}{\partial \theta} \left( \frac{\Gamma}{r} \sin \theta \left( \frac{\partial U}{\partial \theta} + 2V \right) \right)$$

$$+ \rho g_\theta \beta (T - T_{in})$$

$$\text{V-Momentum} \quad \phi = V \quad \Gamma = \mu + \mu_T \quad S\phi = -\frac{\partial p}{\partial r} + \frac{\rho U^2}{r} - \frac{2\Gamma}{r^2} \left( \frac{\partial U}{\partial \theta} + V \right)$$

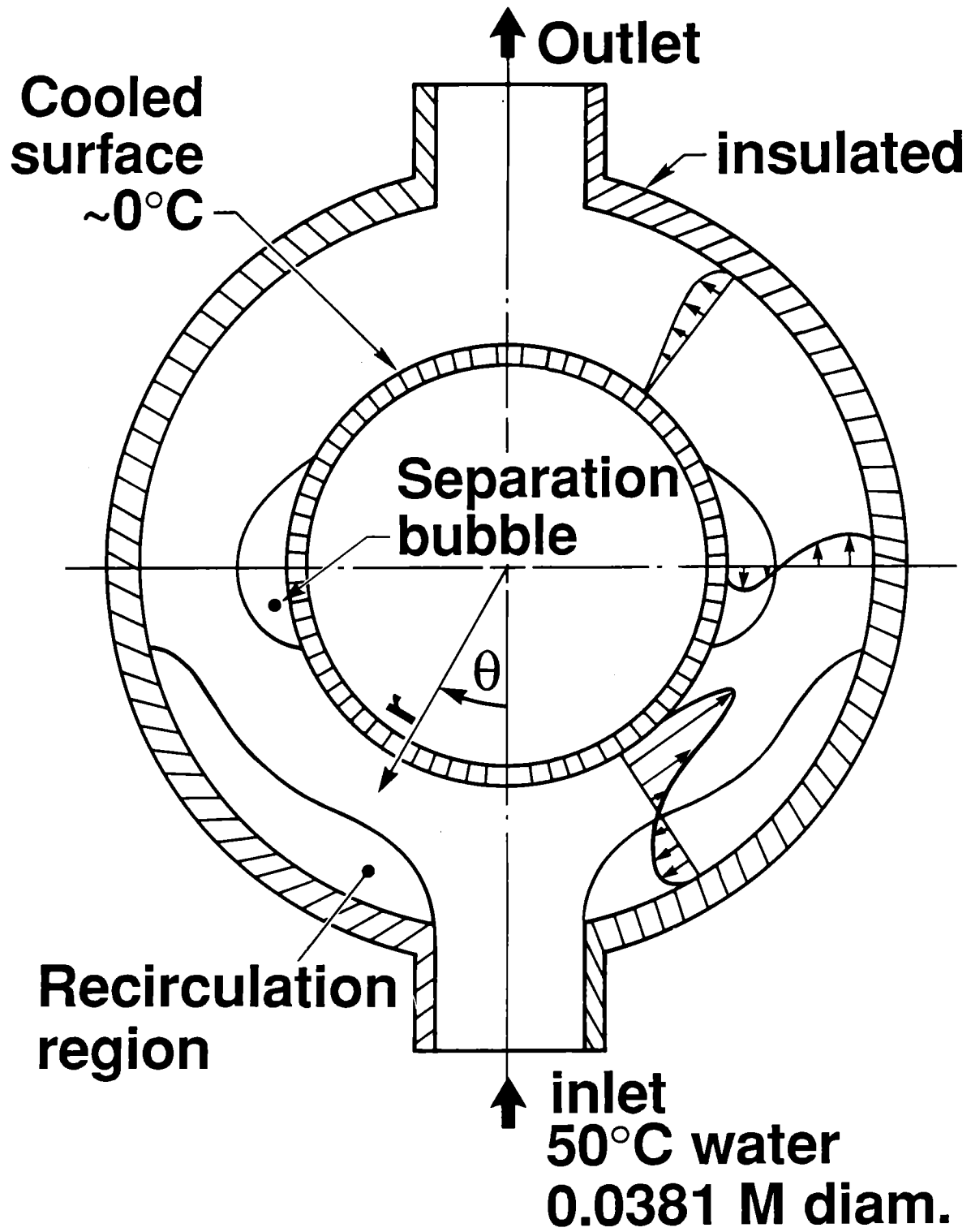
$$+ \frac{1}{r \sin \theta} \frac{\partial}{\partial \theta} \left( r \Gamma \sin \theta \frac{\partial}{\partial r} \left( \frac{U}{r} \right) \right) + \frac{1}{r^2} \frac{\partial}{\partial r} \left( r^2 \Gamma \frac{\partial V}{\partial r} \right) + \rho g_r \beta (T - T_{in})$$

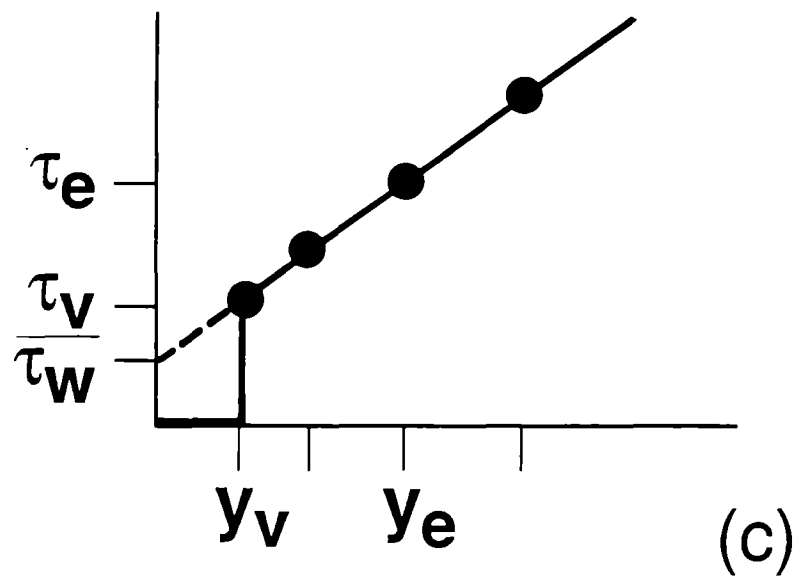
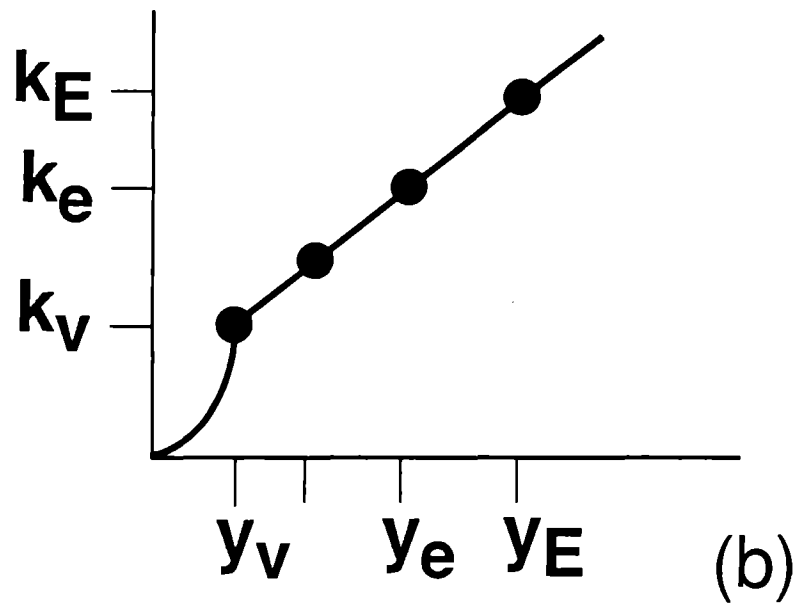
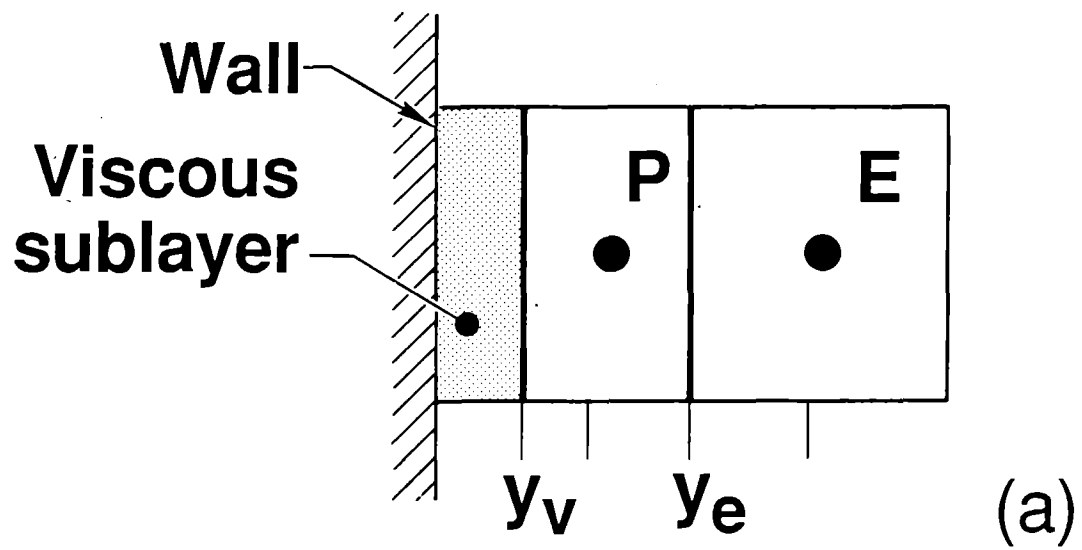
$$\text{where:} \quad \mu_T = \rho c_\mu k^2 / \epsilon$$

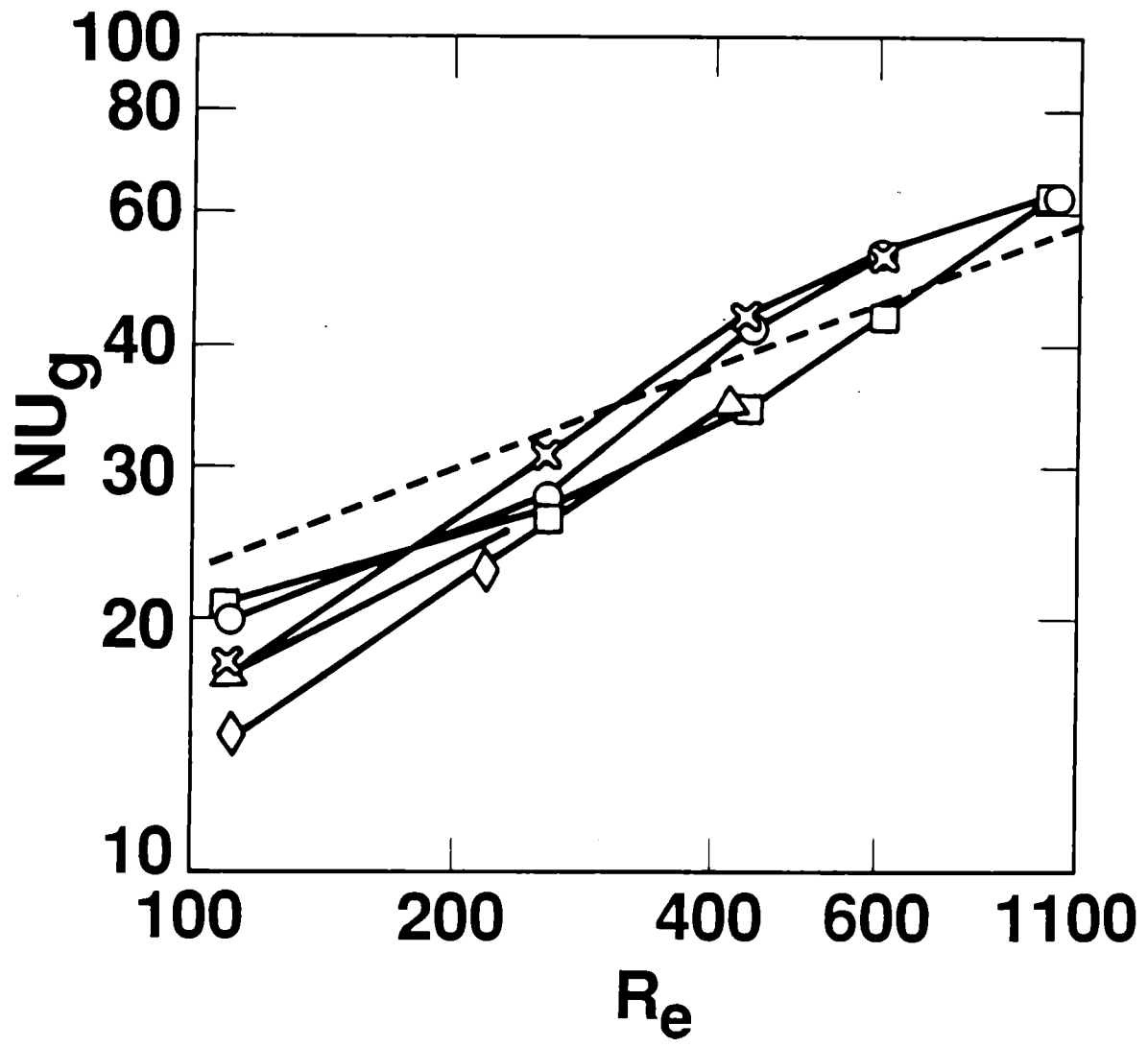
$$P = \mu_T \left[ 2 \left[ \left( \frac{\partial V}{\partial r} \right)^2 + \left( \frac{\partial U}{r \partial \theta} + \frac{V}{r} \right)^2 + \left( \frac{V}{r} + \frac{U}{r} \cot \theta \right)^2 \right] + \left( r \frac{\partial}{\partial r} \left( \frac{U}{r} \right) + \frac{\partial V}{r \partial \theta} \right)^2 \right]$$

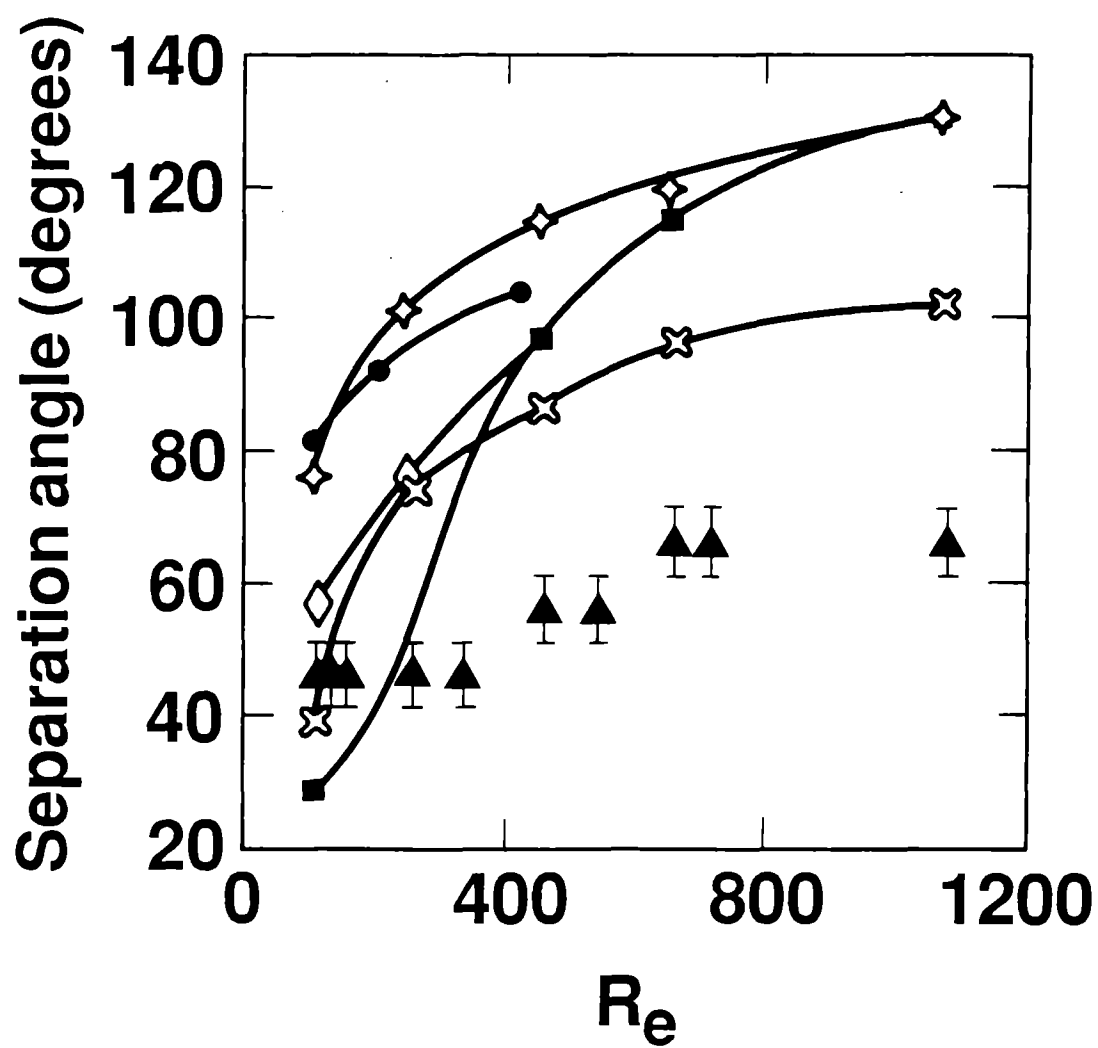
Table 2 Turbulence Model Constants.

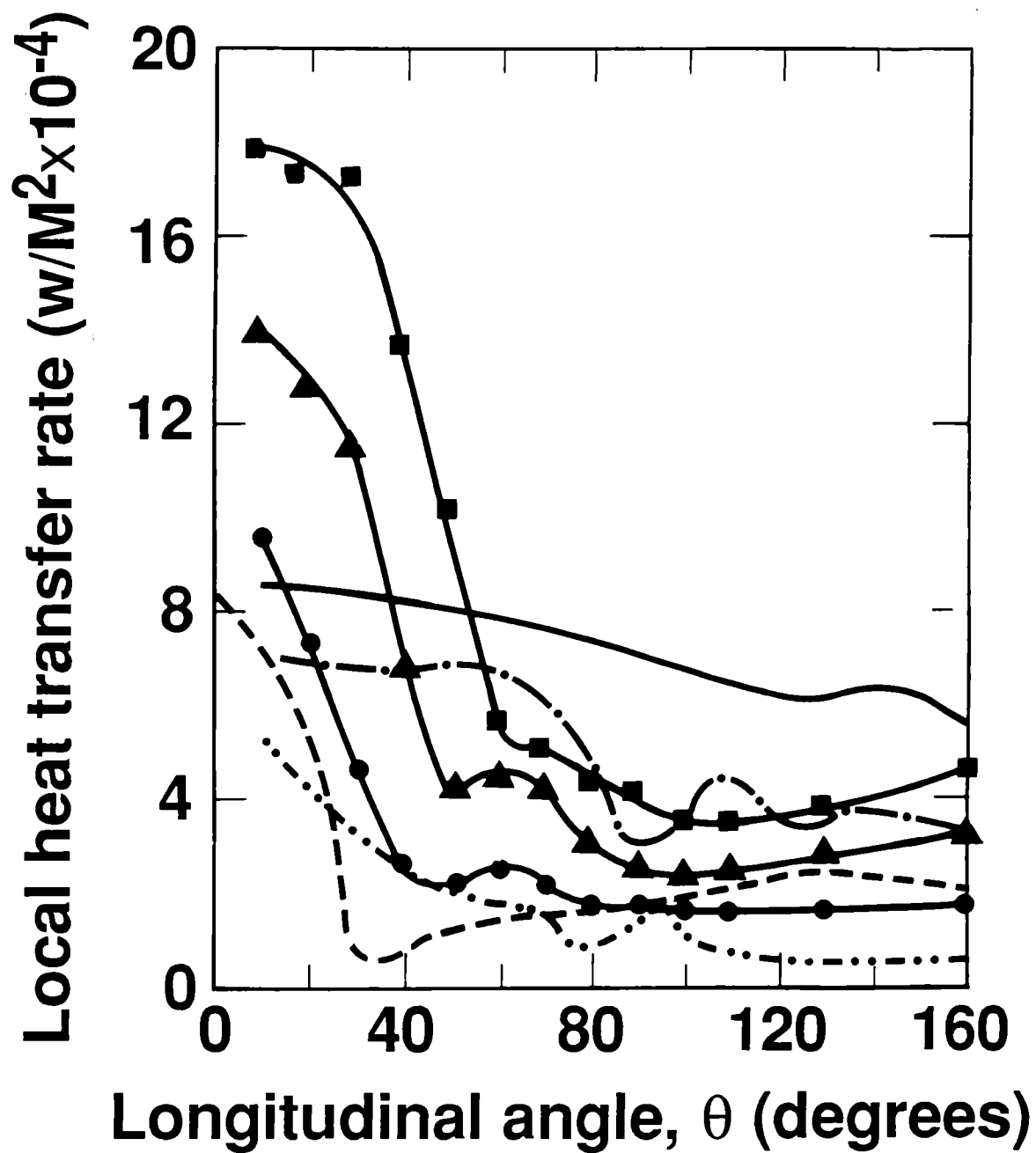
$C_\mu$	$C_1$	$C_2$	$\sigma_k$	$\sigma_\epsilon$	$\sigma_T$
0.09	1.44	1.92	1.0	1.3	0.9

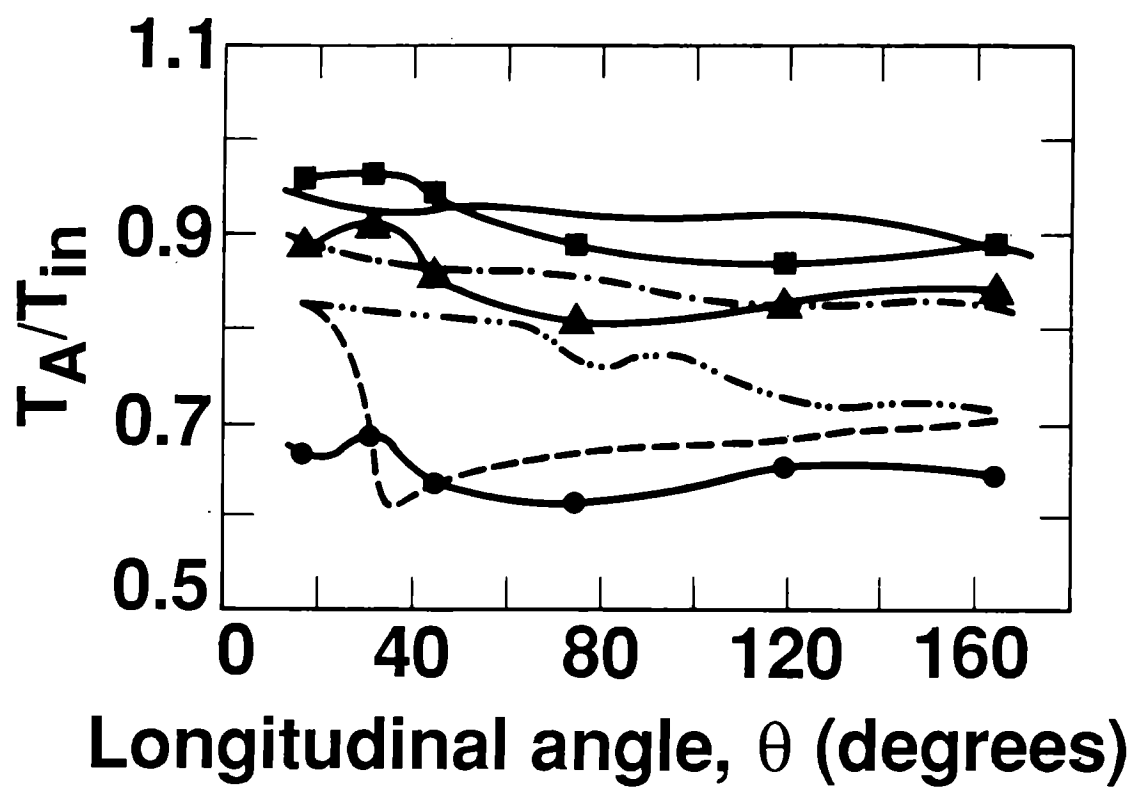


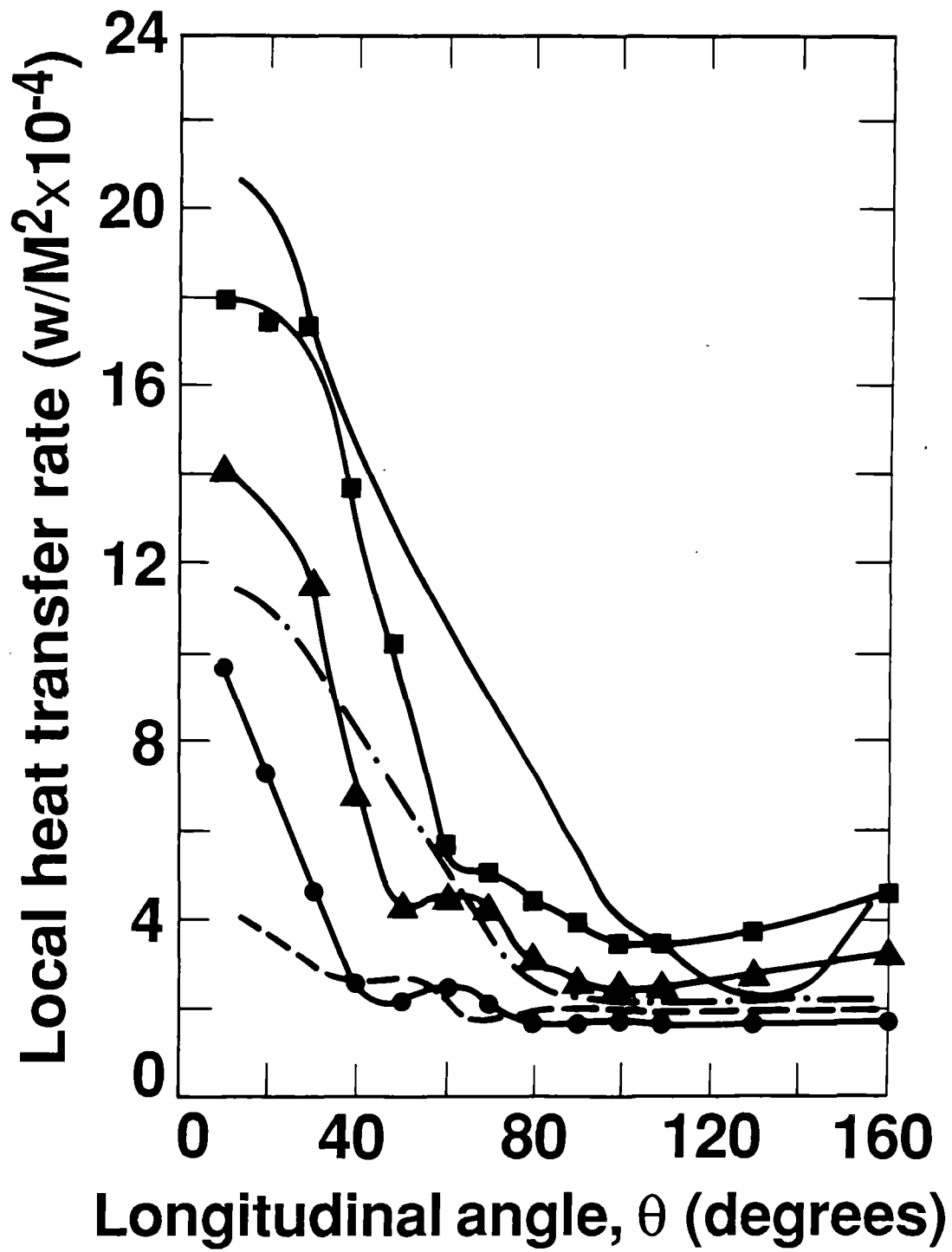


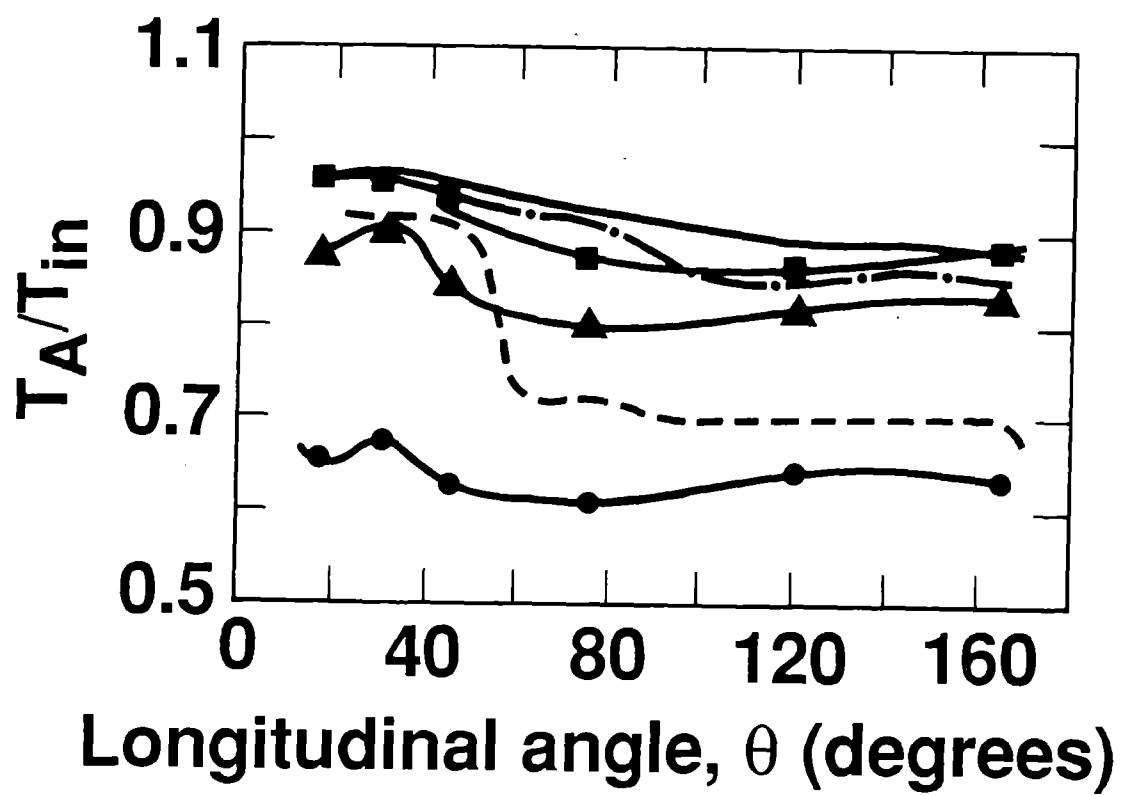


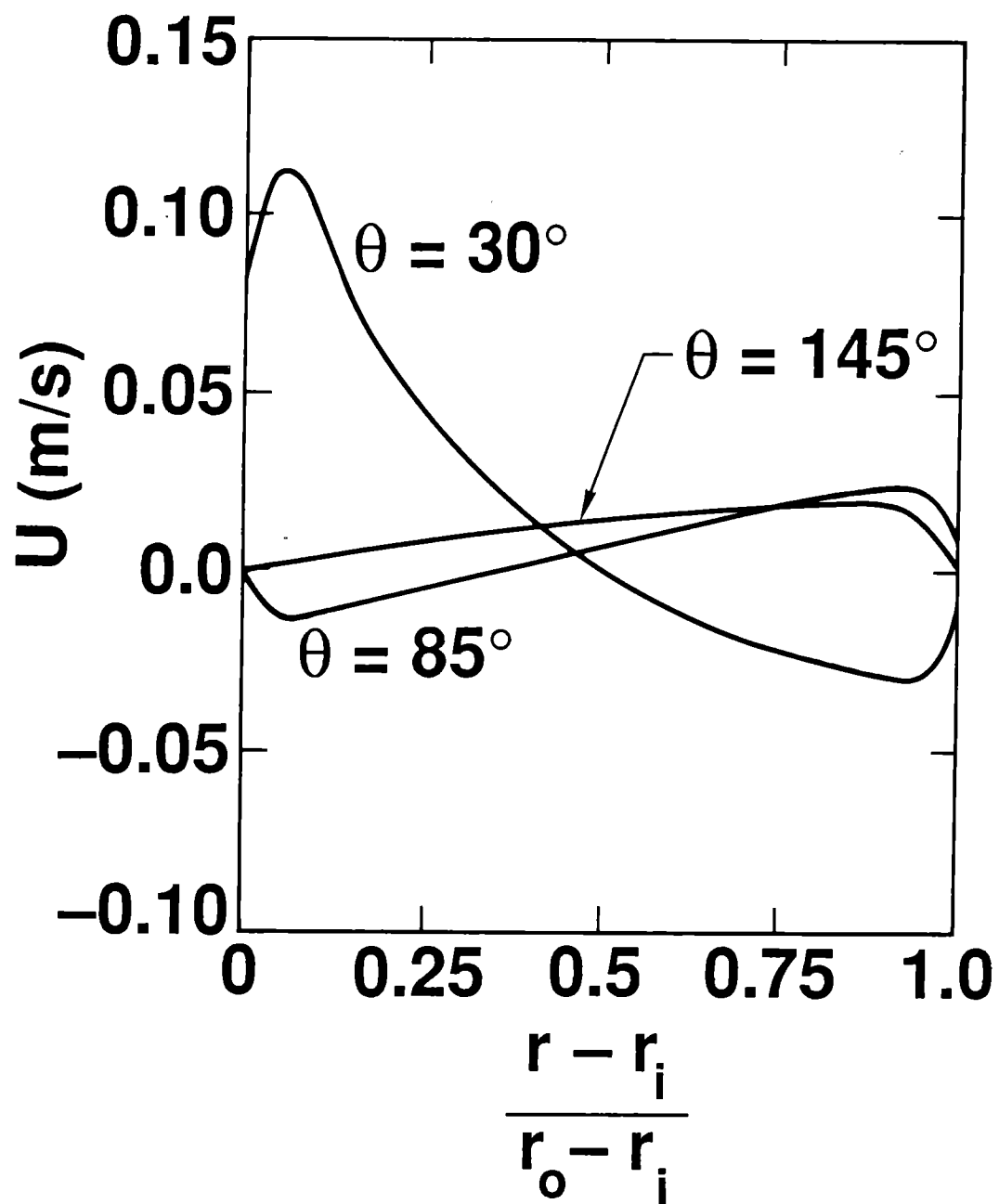












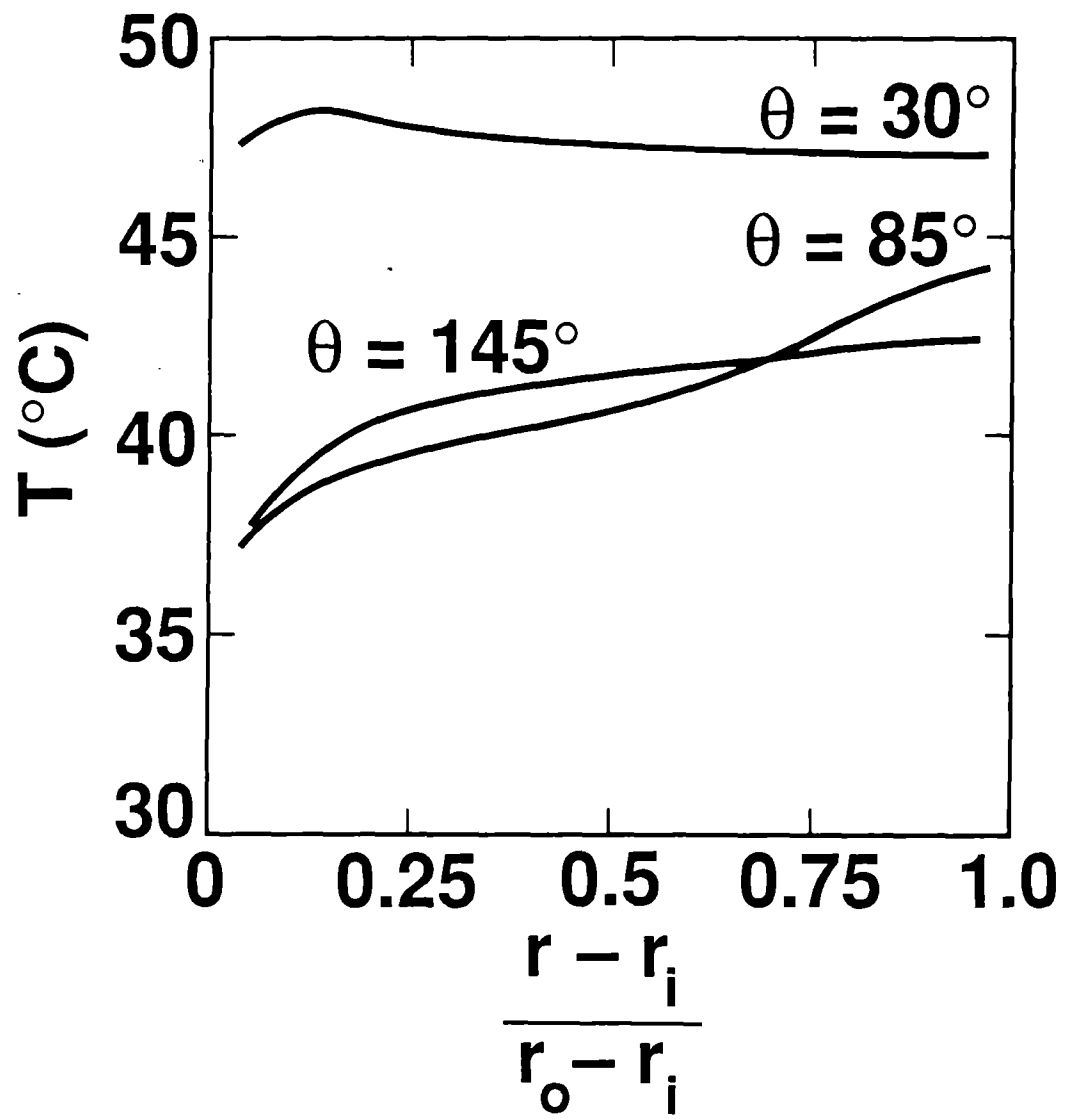


Fig. 1 Geometry of a spherical annulus heat exchanger analyzed and typical flow phenomena computed

Fig. 2 The model for (a) the near wall adjacent cell, (b) the assumed variation of turbulence kinetic energy, and (c) the assumed distribution of turbulent shear stress

Fig. 3 Measured and calculated total-system Nusselt number.  
 ---- Experiment (Tuft and Brandt, 1982). Calculated:  
 ◇ laminar (Tuft and Brandt, 1982); ✕ laminar, non-buoyant; ○ laminar, buoyant; □ k-ε model, buoyant; △ k-ε model, non-buoyant

Fig. 4 Measured and calculated separation angles.  
 ▲ Experiment (Tuft and Brandt, 1982). Calculated:  
 ■ laminar, buoyant; ☆ laminar, non-buoyant; ● laminar, non-buoyant (Tuft and Brandt, 1982); ◇ k-ε model; ✕ mixing length model

Fig. 5 Local heat transfer rate based on a laminar flow calculation. Experiment (Tuft and Brandt, 1982):  
 ■  $Re = 1086$ ; ▲  $Re = 465$ ; ●  $Re = 110$ . Calculated:  
 —  $Re = 1086$ ; -.-  $Re = 465$ ; ---  $Re = 110$ ; ---  $Re = 110$ , non-buoyant

Fig. 6 Normalized radial average annulus water temperature distribution based on a laminar flow calculation. Experiment (Tuft and Brandt, 1982):  
 ■  $Re = 1086$ ; ▲  $Re = 465$ ; ●  $Re = 110$ . Calculated: —  $Re = 1086$ ;  
 -.-  $Re = 465$ ; ---  $Re = 110$ ; ---  $Re = 110$ , non-buoyant

Fig. 7 Local heat transfer rate based on a k-ε turbulence model calculation. Experiment (Tuft and Brandt, 1982):  
 ■  $Re = 1086$ ; ▲  $Re = 465$ ; ●  $Re = 110$ . Calculated:  
 —  $Re = 1086$ ; -.-  $Re = 465$ ; ---  $Re = 110$

Fig. 8 Normalized radial average annulus water temperature distribution based on a k-ε turbulence model calculation. Experiment (Tuft and Brandt, 1982):  
 ■  $Re = 1086$ ; ▲  $Re = 465$ ; ●  $Re = 110$ . Calculated: —  $Re = 1086$ ;  
 -.-  $Re = 465$ ; ---  $Re = 110$

Fig. 9 Horizontal velocity profiles for flow at a gap Reynolds number of 260 at longitudinal coordinates,  $\theta$ , of 30°, 85° and 115°.

Fig. 10 Temperature profiles for flow at a gap Reynolds number of 260 at longitudinal coordinates,  $\theta$ , of 30°, 85° and 115°.